Letters

Coupling Coefficient Estimation in Inductive Power Transfer Systems Through Damped Frequency

Jiayu Zhou, Xiaosheng Wang, *Student Member, IEEE*, C. Q. Jiang, *Senior Member, IEEE*, Yuanshuang Fan, Tianlu Ma, and Jingchun Xiang, *Graduate Student Member, IEEE*

***Abstract*—This letter proposes a novel approach for estimating coupling coefficients in inductive power transfer systems based on damped frequencies. In systems incorporating a voltage load, disturbances can lead to current/power oscillations at a damped frequency due to poorly damping characteristics. By analyzing the damped frequency of the oscillating components of dc-side currents, the coupling coefficient can be accurately determined without the need for wireless communication, additional hardware, and complex calculations. Experimental results demonstrate the effectiveness of the proposed method, which can estimate coupling coefficients within 0.5 ms based on dc-side currents.**

***Index Terms*—Coupling coefficient, damped frequency, estimation, inductive power transfer (IPT).**

I. Introduction

INDUCTIVE power transfer (IPT) systems, utilizing magnetic resonant coupling, have gained significant attention as a wireless charging solution without the need for physical connections. This technology offers notable advantages, including enhanced reliability, safety, and user friendliness. It has found widespread applications in various domains, such as consumer electronics, electric vehicles, and marine transport. Among various topologies, the series–series (SS) compensation topology, featuring a diode rectifier on the pickup side, is widely adopted for inductive battery charging due to its cost-effectiveness and high-power density [1].

To effectively track system maximum efficiency and facilitate model-based controller design, it is essential to have knowledge of the system state, including the coupling coefficient [2], [3]. Previous studies have employed real-time system measurements for coupling calculations, but this approach often relies on wireless communication, introducing complexity and cost. Alternative methods have been proposed to estimate coupling without the need for wireless communication [4], [5], [6], [10]. For instance, an auxiliary inverter on the sending side enables independent coupling estimation [4]. Another approach, as discussed in [5], utilizes pulse density modulation and interharmonics analysis for estimating system coupling. A recent paper [6] involves frequency sweeping for coupling estimation on the sending side. Moreover, Liu et al. [10] present a coupling estimation method based on the fundamental component and higher harmonics of the system on the primary side. However, these methods typically require specific system parameter information, complex calculations, and additional components, such as auxiliary inverters or ac current sensors.

To avoid the aforementioned issues, this letter proposes a novel method for coupling coefficient estimation of IPT systems. In systems with voltage loads, inadequate system damping can lead to current/power oscillations at damped frequencies when a disturbance occurs [7]. This letter establishes a linear relationship between the system's coupling and the damped frequency. Leveraging this relationship, the coupling coefficient can be accurately determined within 0.5 ms by utilizing the dc-side current. The proposed method is independent of the output voltage, avoids wireless communication and complex calculations, and does not require additional ac sensors or circuit components. It is also robust to parameter sensitivity, with little impact from the coil's parasitic resistance and deviations in resonant frequency on both the sides for IPT systems with loose coupling. Experimental validation is provided to verify the effectiveness of the proposed method.

II. Proposed Method for Estimating Coupling

Fig. 1 illustrates the circuit diagram of a standard SS compensated IPT system with a voltage load. The input is represented by a dc voltage, V_{in}, while the system output is directly connected to a battery, modeled as $V_{\mathrm{dc\_out}}$. The input and output dc currents are denoted as $i_{\mathrm{dc\_in}}$ and $i_{\mathrm{dc\_out}}$, respectively. The system includes v_1 (v_2) and i_1 (i_2) as the sending (pickup) voltage and current, respectively. Moreover, it comprises L_1 (L_2) and C_1

Manuscript received 27 March 2024; revised 10 May 2024 and 10 June 2024; accepted 25 June 2024. Date of publication 4 July 2024; date of current version 4 September 2024. This work was supported in part by the Science Technology and Innovation Committee of Shenzhen Municipality, China, under Grant SGDX20210823104003034, in part by the Research Grants Council, Hong Kong, under ECS Grant 21200622 and Grant CRF-YCRG C7003-22Y, and in part by the Chow Sang Sang Group under Grant 9229159. *(Corresponding authors: Yuanshuang Fan; C. Q. Jiang.)*

The authors are with the Department of Electrical Engineering and the State Key Laboratory of Terahertz and Millimeter Waves, City University of Hong Kong, Hong Kong, SAR, China (e-mail: jiayzhou@cityu.edu.hk; xiaoswang9-c@my.cityu.edu.hk; chjiang@cityu.edu.hk; yuansfan@cityu.edu.hk; tianlu.ma@my.cityu.edu.hk; jinxiang2-c@my.cityu.edu.hk).

Color versions of one or more figures in this article are available at https://doi.org/10.1109/TPEL.2024.3423308.

Digital Object Identifier 10.1109/TPEL.2024.3423308

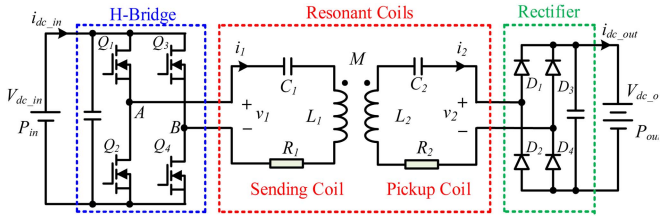

Fig. 1. SS compensated IPT system with a voltage load.

(C_2) as the self-inductance and compensation capacitance for the sending (pickup) side, respectively, along with R_1 (R_2) as the coil's parasitic resistances. The mutual inductance is represented by M. The system parameters typically satisfy the following equation:

$$\omega_r = \frac{1}{\sqrt{L_1 C_1}} = \frac{1}{\sqrt{L_2 C_2}} \tag{1}$$

with ω_r being the system angular resonant frequency.

A. Damped Frequency Analysis Through the Simplified Model

The system depicted in Fig. 1 is typically analyzed using the fundamental harmonic approximation (FHA), assuming sinusoidal waveforms for all the ac voltages and currents. To simplify the analysis and effectively handle rapidly changing state variables, ac signals can be converted into *dq*-axis steady-state variables by establishing a synchronous reference frame. The *d*- and *q*-axis state variables can be interpreted as the real and imaginary components of a dynamic phasor model. Based on Kirchhoff's law, the nonlinear models of the system can be expressed as follows [7]:

$$\begin{aligned}
\frac{di_{1,d}}{dt} &= \omega_s \cdot i_{1,q} - \frac{R_1}{L_{\alpha1}} \cdot i_{1,d} - \frac{MR_2}{L_{\alpha1}L_2} \cdot i_{2,d} - \frac{1}{L_{\alpha1}} \cdot v_{C1,d} \\
&\quad - \frac{M}{L_{\alpha1}L_2} \cdot v_{C2,d} + \frac{1}{L_{\alpha1}} \cdot v_{1,d} - \frac{M}{L_{\alpha1}L_2} \cdot v_{2,d} \\
\frac{di_{1,q}}{dt} &= -\omega_s \cdot i_{1,d} - \frac{R_1}{L_{\alpha1}} \cdot i_{1,q} - \frac{MR_2}{L_{\alpha1}L_2} \cdot i_{2,q} - \frac{1}{L_{\alpha1}} \cdot v_{C1,q} \\
&\quad - \frac{M}{L_{\alpha1}L_2} \cdot v_{C2,q} + \frac{1}{L_{\alpha1}} \cdot v_{1,q} - \frac{M}{L_{\alpha1}L_2} \cdot v_{2,q} \\
\frac{di_{2,d}}{dt} &= \omega_s \cdot i_{2,q} - \frac{MR_1}{L_{\alpha2}L_1} \cdot i_{1,d} - \frac{R_2}{L_{\alpha2}} \cdot i_{2,d} - \frac{M}{L_{\alpha2}L_1} \cdot v_{C1,d} \\
&\quad - \frac{1}{L_{\alpha2}} \cdot v_{C2,d} + \frac{M}{L_{\alpha2}L_1} \cdot v_{1,d} - \frac{1}{L_{\alpha2}} \cdot v_{2,d} \\
\frac{di_{2,q}}{dt} &= -\omega_s \cdot i_{2,d} - \frac{MR_1}{L_{\alpha2}L_1} \cdot i_{1,q} - \frac{R_2}{L_{\alpha2}} \cdot i_{2,q} - \frac{M}{L_{\alpha2}L_1} \cdot v_{C1,q} \\
&\quad - \frac{1}{L_{\alpha2}} \cdot v_{C2,q} + \frac{M}{L_{\alpha2}L_1} \cdot v_{1,q} - \frac{1}{L_{\alpha2}} \cdot v_{2,q} \\
\frac{dv_{c1,d}}{dt} &= \omega_s \cdot v_{c1,q} + \frac{1}{C_1} \cdot i_{1,d} \quad \frac{dv_{c1,q}}{dt} = -\omega_s \cdot v_{c1,d} + \frac{1}{C_1} \cdot i_{1,q} \\
\frac{dv_{c2,d}}{dt} &= \omega_s \cdot v_{c2,q} + \frac{1}{C_2} \cdot i_{2,d} \quad \frac{dv_{c2,q}}{dt} = -\omega_s \cdot v_{c2,d} + \frac{1}{C_2} \cdot i_{2,q}
\end{aligned} \tag{2}$$

where $L_{\alpha1} = L_1 - M^2/L_2$, $L_{\alpha2} = L_2 - M^2/L_1$, and ω_s represents the angular switching frequency of the system.

In the dynamic phasor model of IPT systems, the resonant capacitor can be approximated as an equivalent inductor to simplify the system and reduce its complexity at ω_s. Therefore, (2) can be simplified to the following equation [8]:

$$\begin{cases}
\frac{di_{1d}}{dt} = (\omega_s - \omega_r) i_{1q} - \frac{R_1 \omega_s i_{1,d}}{(\omega_s+\omega_r)L_1} + \frac{\omega_s^2 M i_{2,q}}{(\omega_s+\omega_r)L_1} + \frac{\omega_s v_{1d}}{(\omega_s+\omega_r)L_1} \\
\frac{di_{1q}}{dt} = -(\omega_s - \omega_r) i_{1d} - \frac{R_1 \omega_s i_{1,q}}{(\omega_s+\omega_r)L_1} - \frac{\omega_s^2 M i_{2,d}}{(\omega_s+\omega_r)L_1} + \frac{\omega_s v_{1q}}{(\omega_s+\omega_r)L_1} \\
\frac{di_{2d}}{dt} = (\omega_s - \omega_r) i_{2q} - \frac{R_2 \omega_s i_{2d}}{(\omega_s+\omega_r)L_2} + \frac{\omega_s^2 M i_{1q}}{(\omega_s+\omega_r)L_2} + \frac{\omega_s v_{2d}}{(\omega_s+\omega_r)L_2} \\
\frac{di_{2q}}{dt} = -(\omega_s - \omega_r) i_{2d} - \frac{R_2 \omega_s i_{2q}}{(\omega_s+\omega_r)L_2} - \frac{\omega_s^2 M i_{1d}}{(\omega_s+\omega_r)L_2} + \frac{\omega_s v_{2q}}{(\omega_s+\omega_r)L_2}.
\end{cases} \tag{3}$$

To minimize reactive power and achieve high efficiency, the system typically operates at the resonant frequency ($\omega_s = \omega_r$), satisfying the following relationship [9]:

$$\begin{cases}
v_{1d}(t) = V_1; v_{1q}(t) = 0; i_{1q}(t) = i_{2d}(t) = 0; v_{2d}(t) = 0; \\
v_{2q}(t) = V_2 \\
I_1(t) = \sqrt{i_{1d}^2(t) + i_{1q}^2(t)} = i_{1d}(t)
\end{cases} \tag{4}$$

where I_1 is the envelope of the sending current.

Solving (3) and (4) allows for obtaining the envelope of the sending current (I_1), expressed in the *s* domain

$$I_1(s) = \frac{\left(2L_2V_1 s + \omega_r M V_2 + R_2 V_1\right)/(4L_1L_2)}{s^2 + \left((2L_1R_2 + 2L_2R_1)/(4L_1L_2)\right) s + (\omega_r^2 M^2 + R_1R_2)/4L_1L_2}. \tag{5}$$

The response of I_1 can be viewed as a second-order system, and its angular natural frequency (ω_n) can be expressed as follows:

$$\omega_n^2 = \frac{\omega_r^2 M^2 + R_1R_2}{4L_1L_2} \xrightarrow{\omega_r^2 M^2 \gg R_1R_2} k = \frac{M}{\sqrt{L_1L_2}} \approx \frac{2\omega_n}{\omega_r} \tag{6}$$

where k is the coupling coefficient. The aforementioned equation reveals a linear relationship between the angular natural frequency ω_n of $I_1(t)$ and the coupling coefficient k. Therefore, this property can be utilized to estimate the coupling coefficient of the system in a straightforward and effective manner. However, obtaining the natural frequency of $I_1(t)$ can be challenging in practical applications, while measuring the damped frequency is relatively simpler. Moreover, in IPT systems with voltage load, the damping is typically low at the resonant frequency [7]. Therefore, the angular damped frequency (ω_d) of the system can be calculated using the following equation in low-damping systems:

$$\omega_d = \left(\sqrt{1 - \xi^2}\right) \omega_n \approx \omega_n \tag{7}$$

where ξ is the system damping. The proposed method leverages the damped frequency of the current amplitude to calculate the coupling coefficient. By utilizing (6) and (7), coupling estimation can be achieved without the need for wireless communication, additional hardware, or complex computations.

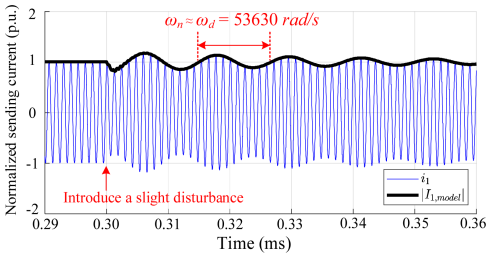

Fig. 2. Response of sending current under small perturbation when $k = 0.2$.

TABLE I
PARAMETERS OF THE IPT SYSTEM

General parameters	Values
Input voltage, V_{dc_in}	25 V
Output voltage, V_{dc_out}	25 V
Angular resonant frequency, ω_r	534 000 rad/s
Self-inductance, L_1, L_2	57, 57 μH
Coil's parasitic resistance, R_1, R_2	0.05, 0.05 Ω

B. Sensitivity Analysis of the Proposed Method

Equation (6) provides insight into the relationship between the natural frequency of $I_1(t)$ and coupling. However, the calculation process for the reduced-order model presented in (3) is an approximation [8]. To validate the results obtained from (6) and evaluate the impact of system parameters, the full-order nonlinear model described in (2) is used. When a small perturbation is introduced to the system, Fig. 2 presents the sending current's response with a coupling value of 0.2, using the parameters in Table I. The blue line represents the sending current, $i_1(t)$, obtained from the circuit model through MATLAB/Simulink, while the black line represents the sending current amplitude, $I_1(t)$, calculated from the nonlinear model shown in (2). At $t = 0.3$ ms, the input voltage momentarily drops to zero for half a switching cycle. It is evident that the outcomes derived from the full-order model align with the results obtained from the circuit model. Moreover, $I_1(t)$ exhibits small-amplitude oscillations with an angular damped frequency of 53 630 rad/s. Utilizing (6) and (7), the estimated coupling of the system is approximately 0.201, with an estimation error within 1%. This initial validation demonstrates the effectiveness of the proposed method. Notably, the pickup-side current amplitude, which exhibits the same damped frequency due to the inherent properties of the system, can also be used to estimate the coupling.

To verify the proposed method's applicability, the impact of system parameter deviations on coupling estimation should be analyzed. By using parameters in Table I, Fig. 3 presents the natural frequency and damping results for $I_1(t)$, obtained from linearizing the model shown in (2) with parameter deviations, including variations in output voltage, parasitic resistances, and detuning factor x_c [defined as $C_1L_1/(C_2L_2)$]. Fig. 3(a) demonstrates that the output voltage has no effect on natural frequency and damping of $I_1(t)$, aligning with (6). Thus, wireless communication is unnecessary as the proposed method remains unaffected by the output voltage values. Moreover, different parasitic resistance values are examined in Fig. 3(b), observing

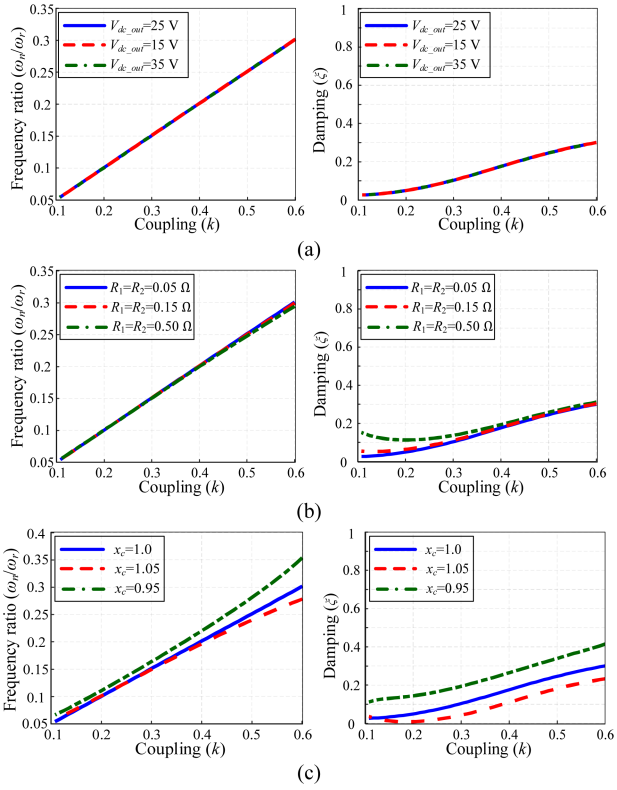

Fig. 3. Natural frequency and damping of $I_1(t)$ with changing coupling in the IPT system. (a) Variation with different output voltage loads. (b) Variation with different parasitic resistance. (c) Variation with different detuning factors x_c.

negligible impact on the natural frequency of current amplitude, even when $R_{1(2)}$ is increased tenfold. While damping increases notably at low coupling, it remains below 0.2, with minor influence on damped frequency and natural frequency deviations as (7). Moreover, Fig. 3(c) illustrates the sensitivity of the proposed method to resonant frequency deviations. As x_c deviates from 1.0, the error increases with an increasing value of k. Moreover, it is noted that for $x_c > 1$, the error may be relatively smaller compared to $x_c < 1$. Generally, x_c is designed slightly above 1 for achieving zero-voltage switching but usually below 1.05 for maintaining high coil efficiency [1]. Based on the aforementioned analysis, the proposed method is highly robust and relatively unaffected by system parameter deviations in conventionally designed IPT systems.

C. Implementation of Coupling Coefficient Identification

Estimating the system coupling through the damped frequency of $I_1(t)$ is feasible, but accurately obtaining the envelope of ac currents is often challenging. Moreover, the system typically measures the dc-side voltage and current for power regulation. To avoid the need for additional ac current sensors, such as $i_1(t)$, the damped frequency of the oscillating part of the input dc current $i_{dc\_in}(t)$ can be directly measured for coupling estimation, as the system exhibits the same damped frequency shown in Fig. 4. When a disturbance occurs, the ac-side current amplitude will oscillate at the damped frequency based on (5). In this scenario, the system's current can be expressed using the

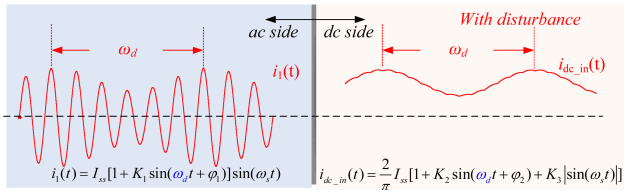

Fig. 4. Relationship between AC- and DC-side currents in presented systems with disturbance.

following equation [11]:

$$\begin{cases} i_1(t) = I_{\rm ss}[1 + K_1 \sin(\omega_d t + \varphi_1)] \sin(\omega_s t) \\ i_{\rm dc\_in}(t) = \frac{2}{\pi} I_{\rm ss}[1 + K_2 \sin(\omega_d t + \varphi_2) + K_3 \,|\sin(\omega_s t)|] \end{cases} \tag{8}$$

where $I_{\rm ss}$ is the ac current amplitude value of the system in the steady state. The coefficients $K_{1(23)}$ and $\varphi_{1(2)}$ represent the amplitude and phase angle of the current oscillation, respectively, which are influenced by system parameters and the applied perturbation. It is worth noting that filter components, such as dc-link capacitors, primarily influence the phase and amplitude of the current oscillation, while the damped frequency used in the proposed method remains unaffected by these components. To maintain the desired steady-state operating point, a practical solution involves skipping one pulse in the sending-side converter. This approach effectively introduces a perturbation and triggers current oscillations at the damped frequency. Therefore, the proposed method enables fast coupling estimation in IPT systems without requiring wireless communication. Moreover, this approach leverages the existing dc-side current sensor within the system, eliminating the necessity for additional components and complex calculations. It is worth noting that ω_d of the dc current oscillation component can be obtained in the digital controller. To accurately extract the oscillation component, the dc current can undergo bandpass filtering, effectively filtering out the dc and switching frequency components. It is clarified that the amplitude and phase of the oscillation component are not crucial, as the main focus is on measuring the frequency of the oscillation component. This measurement is not affected by the AD sampling delay or the bandpass filter. Moreover, the digital controller performs zero-crossing detection on the filtered current by detecting the sign bit of the filtered data. By calculating the time difference between two consecutive rising zero crossings, the damped frequency of the current oscillation component can be determined. This allows for an accurate estimation of the system's damped frequency in practical applications.

III. Experimental Verification

A laboratory prototype, depicted in Fig. 5, was constructed to validate the proposed coupling estimation method, with system specifications listed in Table I. Fig. 6 presents the experimental results of the system with a coupling coefficient of 0.203. At time t_1, an input pulse is skipped, leading to small-amplitude oscillations observed in dc-side currents. By measuring the time difference between the peak values of the oscillation, the angular damped frequency of the system is determined to

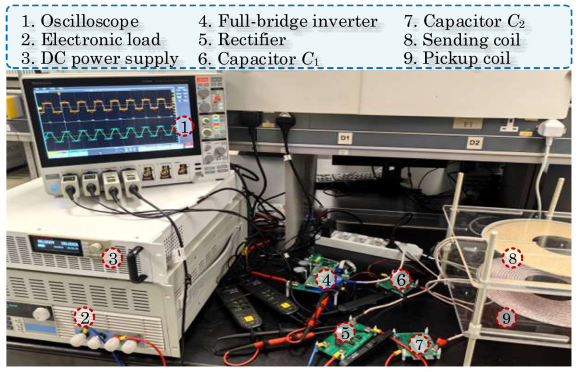

Fig. 5. Prototype of the IPT system.

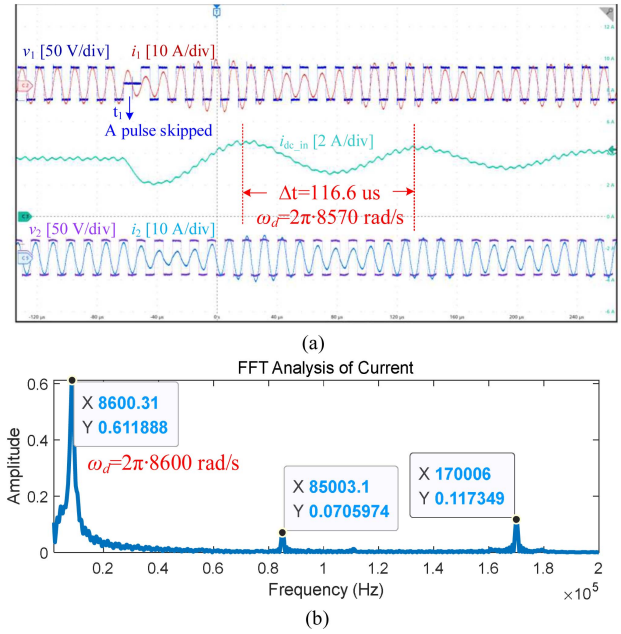

Fig. 6. Experimental results when k is 0.203. (a) Waveforms. (b) FFT analysis of the oscillating components in input DC-side current.

be $2\pi \cdot 8570$ rad/s. Utilizing (6) and (7), the coupling can be estimated to be 0.202, which closely matches the actual coupling value within a 1% margin. Moreover, fast Fourier transform analysis on the oscillation components of the dc-side current in Fig. 6(b) further confirms the accuracy of the proposed method. Therefore, coupling estimation can be accomplished within a few switching cycles, while the disturbance caused does not affect the system's steady-state operation, returning to normal within 2 ms.

Fig. 7 presents the experimental results when the system parameters deviate from Table I. Since the output voltage changes gradually during battery charging, the coupling estimation results are showcased for two different output voltages of 15 and 35 V, resulting in estimated couplings of 0.204 and 0.203, respectively, both with errors within 1%. To examine the effect of coil parasitic resistances, additional resistors ($R = 0.2\ \Omega$ and $R = 0.5\ \Omega$) were added to the primary and secondary sides of the circuit. The experimental results, depicted in Fig. 7(c) and (d),

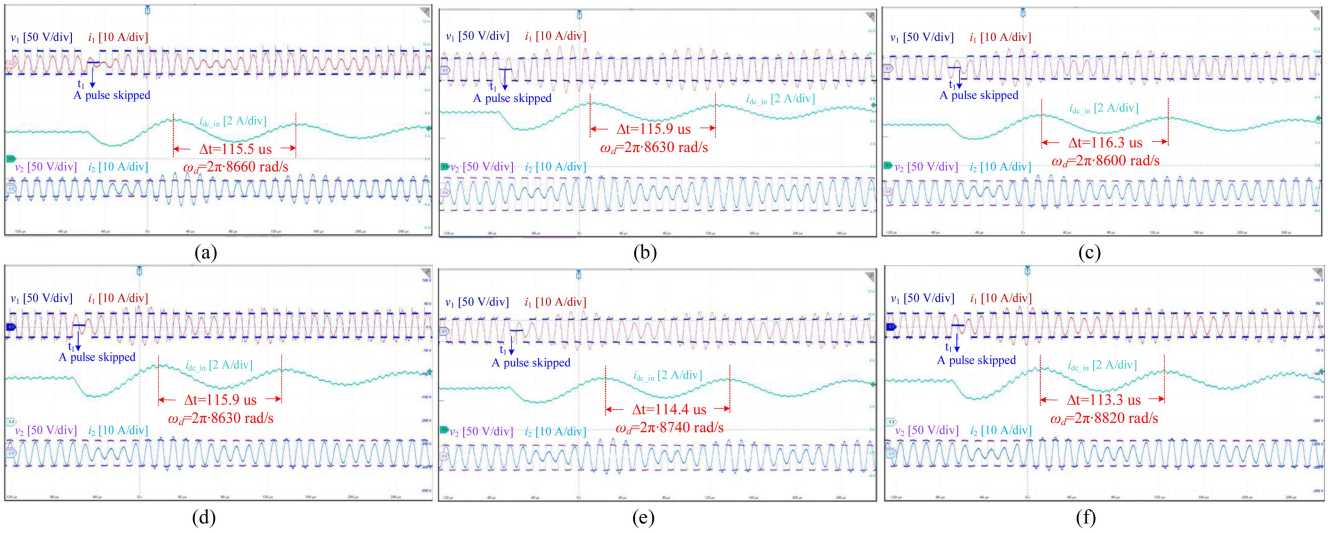

Fig. 7. Experimental results for parameter deviation from rated parameters when k is 0.203. (a) $V_{\mathrm{dc\_out}} = 15$ V. (b) $V_{\mathrm{dc\_out}} = 35$ V. (c) $R_1 = R_2 = 0.25\ \Omega$. (d) $R_1 = R_2 = 0.55\ \Omega$. (e) $x_c = 0.95$. (f) $x_c = 1.05$.

demonstrate that the coupling estimation is minimally affected. The estimated couplings for these scenarios are 0.202 and 0.203, respectively, with errors within 1%. Moreover, deviations that may occur during the mass production of resonant tanks were considered. Experiments were conducted by increasing the secondary-side resonant capacitance value to $x_c = 0.95$ and increasing the primary-side resonant capacitance value to $x_c = 1.05$. Fig. 7(e) and (f) presents the results for these two cases. It is observed that the damped frequencies of the system slightly increased, resulting in estimated couplings of 0.206 and 0.208, with errors within 3%. Therefore, the proposed method exhibits high accuracy and is not sensitive to parameter changes during loose coupling, making it highly suitable for practical implementation.

To further demonstrate the results, the rising zero-crossing detection signal captured by the field-programmable gate array (FPGA) controller is presented on the oscilloscope, as shown in Fig. 8. When the system performs online coupling estimation, a pulse is skipped. The dc-side current then starts to oscillate at the damped frequency and stabilizes within 2 ms. The FPGA-detected rising zero-crossing signal is also shown on the oscilloscope. It can be observed that the coupling estimation is completed within 0.2 ms, and the estimated result of 0.207, calculated from the damped frequency, is within 2% of the actual value of 0.203. The zero-crossing point determined by the FPGA is slightly delayed compared to the actual current oscillation zero-crossing time. This is mainly due to the AD sampling delay and the filtering process. However, these factors do not affect the measurement of the damped frequency of the oscillation component. It is important to highlight that only one coupling estimation is performer for each skipped pulse. While there may be additional zero-crossing points of the current oscillation component later, they will not be detected. The FPGA controller will only perform zero-crossing detection and coupling estimation again when a new estimation instruction is issued, and a pulse is skipped.

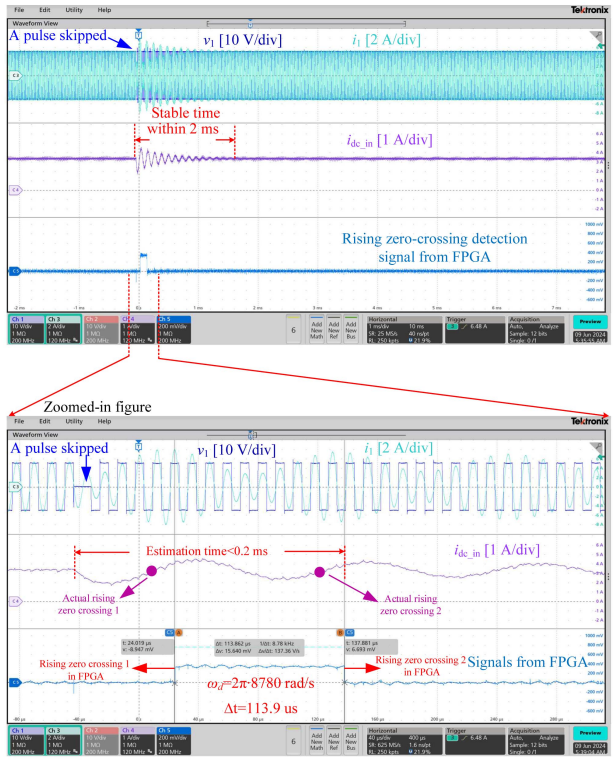

Fig. 8. Experimental results of online coupling estimation when k is 0.203.

Fig. 9 illustrates the estimation results obtained using the proposed method for various coupling coefficients. When the coupling is less than 0.4, the method exhibits high accuracy with errors below 3%. It should be noted that the proposed method may not be suitable for high coupling situations due to increased damping, and the analyses in this letter, which rely on FHA and disregard higher harmonics, may lead to increasing errors at high coupling.

TABLE II
COMPARISON OF DIFFERENT COUPLING ESTIMATION METHODS

References	Maximum error	Estimation time	Auxiliary circuit or current sensor	Calculation	Wireless communication	Other characteristics
[2]	8%	300 ms	Additional dc–dc converters	Intermediate	Yes	Dynamic coupling estimation
[4]	6%	–	Auxiliary inverter and one ac current sensor	Complex	No	Operates at or near the resonant frequency
[5]	5%	2–5 s	One ac current sensor	Highly complex	No	Applies in pulse density modulation
[6]	6.8%	2 ms	One ac current sensor	Complex	No	Requires frequency sweeping and cannot operate at receiver resonant frequency
[10]	6.9%	7 ms	One ac current sensor	Highly complex	No	Utilizes harmonic analysis and suitable for different topologies
This letter	5%	<0.5 ms	One dc current sensor	Simple	No	Operates at or near the resonant frequency

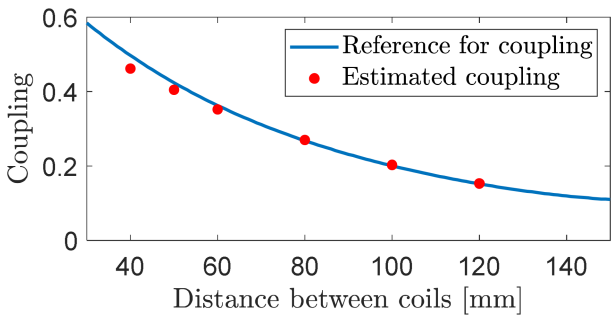

Fig. 9. Estimation results of the proposed method.

Table II provides a comparison between the proposed method and the existing state-of-the-art coupling estimation methods. The table includes several classic approaches, such as those utilizing auxiliary circuits [4], subharmonics [5], frequency sweeps [6], and high-order harmonics [10]. One notable advantage of the proposed method is its remarkably short settling time, which falls within 0.5 ms. Moreover, it eliminates the need for additional hardware or ac current sensors while also significantly reducing the computational effort needed. The short coupling estimation time depicted in Fig. 8 indicates the potential of the proposed method to perform the real-time online estimation of dynamic coupling changes, as long as the coupling variations are not too rapid. However, it is essential to acknowledge certain limitations. The method cannot issue coupling estimation instructions too frequently because each estimation trigger induces small oscillations in the system that persists for approximately 1 ms. Moreover, the proposed method is primarily suitable for systems operating at the resonant frequency.

IV. CONCLUSION

This letter proposes a novel approach for the rapid estimation of the coupling coefficient in IPT systems using the dc-side current, without the need for wireless communication, additional components, or complex calculations. By intentionally skipping a modulated pulse of the converter, which acts as a disturbance, the system undergoes slight oscillations at the damped frequency, including dc currents on both the sides. By establishing the linear relationship between coupling and damped frequency, the proposed method enables rapid and accurate estimation of system coupling. The effectiveness of the proposed method has been confirmed through simulations and experimental results.

REFERENCES

[1] G. Guidi and J. A. Suul, "Minimizing converter requirements of inductive power transfer systems with constant voltage load and variable coupling conditions," *IEEE Trans. Ind. Electron.*, vol. 63, no. 11, pp. 6835–6844, Nov. 2016.
[2] X. Dai, X. Li, Y. Li, and A. Hu, "Maximum efficiency tracking for wireless power transfer systems with dynamic coupling coefficient estimation," *IEEE Trans. Power Electron.*, vol. 33, no. 6, pp. 5005–5015, Jun. 2018.
[3] W. Li, G. Wei, C. Cui, X. Zhang, and Q. Zhang, "A double-side self-tuning LCC/S system using a variable switched capacitor based on parameter recognition," *IEEE Trans. Ind. Electron.*, vol. 68, no. 4, pp. 3069–3078, Apr. 2021.
[4] X. Sheng and L. Shi, "Mutual inductance and load identification method for inductively coupled power transfer system based on auxiliary inverter," *IEEE Trans. Veh. Technol.*, vol. 69, no. 2, pp. 1533–1541, Feb. 2020.
[5] R. Dai, W. Zhou, Y. Chen, Z. Zhu, and R. Mai, "Pulse density modulation based mutual inductance and load resistance identification method for wireless power transfer system," *IEEE Trans. Power Electron.*, vol. 37, no. 8, pp. 9933–9943, Aug. 2022.
[6] J. Zeng, J. Wu, K. Li, Y. Yang, and S. Y. R. Hui, "Dynamic monitoring of battery variables and mutual inductance for primary-side control of a wireless charging system," *IEEE Trans. Ind. Electron.*, vol. 71, no. 7, pp. 7966–7974, Jul. 2024.
[7] J. Zhou, G. Guidi, K. Ljøkelsøy, and J. A. Suul, "Evaluation and suppression of oscillations in inductive power transfer systems with constant voltage load and pulse skipping modulation," *IEEE Trans. Power Electron.*, vol. 38, no. 8, pp. 10412–10425, Aug. 2023.
[8] H. Li, J. Fang, and Y. Tang, "Dynamic phasor-based reduced-ordermodels of wireless power transfer systems," *IEEE Trans. Power Electron.*, vol. 34, no. 11, pp. 11361–11370, Nov. 2019.
[9] Y. Zhang, X. Li, S. Chen, and Y. Tang, "Soft switching for strongly coupled wireless power transfer system with 90° dual-side phase shift," *IEEE Trans. Ind. Electron.*, vol. 69, no. 1, pp. 282–292, Jan. 2022.
[10] J. Liu, G. Wang, G. Xu, J. Peng, and H. Jiang, "A parameter identification approach with primary-side measurement for DC–DC wireless-power-transfer converters with different resonant tank topologies," *IEEE Trans. Transp. Electrific.*, vol. 7, no. 3, pp. 1219–1235, Sep. 2021.
[11] R. W. Erickson and D. Maksimovic, *Fundamentals of Power Electronics*. Berlin, Germany: Springer, 2007.